Structure and domain formation in ferroelectric thin films

Vlooswijk, Ard H.G.

Chapter 2

State of the art of ferroelectrics

2.1 Introduction

Although the macroscopic understanding of the classical ferroelectric $PbTiO_3$ is to a large extent established, the behavior on the atomistic level and close to the phase transition, is not. This applies even more to the solid-solutions with $PbTiO_3$ as the "parent compound", often used in applications. Indeed, many ferroelectrics used in devices are $PbTiO_3$-based solid solutions with the other end member of the solid solution chosen such that a phase boundary nearly parallel to the temperature axis exists between different crystallographic phases, the so-called "Morphotropic Phase Boundary" (MPB; see Figure 1.6). Ultrahigh piezoelectric coefficients and electromechanical coupling factors are observed close to this MPB. The cause of the enhanced piezoelectric properties of these materials is not yet fully understood and different models exist to explain the behavior. Most explanations are related to the behavior of the "parent compound" under (chemical) pressure or in electric field, but a unified theory is not yet established. The interplay between theory and experiment on "parent compounds" and solid solutions is leading to an increased insight into the important mechanisms underlying the enhanced piezoelectric response. But real bulk systems are far from the ideal materials considered in the theory. Epitaxially strained and (partially) relaxed thin films of $PbTiO_3$ could lead to more insight in the suitability of the different models.

This chapter gives a description of the atomistic mechanisms of ferroelectricity in $PbTiO_3$ and the models to explain the enhanced piezoelectric properties of solid solutions, as well as the theoretical approaches to describe ferroelectric thin films under epitaxial strain. These descriptions can generally be attempted in two ways: First principles calculations which are purely theoretical (as long as ab initio parameters are used), on the one side, and

phenomenological calculations, which involve a descriptive approach, on the other side. First, we consider the mechanism of ferroelectricity in bulk ferroelectrics. Subsequently, we show how the theory and phenomenology can be modified to be applied to epitaxial thin films. Finally, we will list the driving forces for the appearance of ferroelectric domains in these thin films and the way these domain structures self-organize.

2.2 Classical ferroelectrics and solid solutions

$PbTiO_3$ is an archetype of tetragonal perovskite ferroelectrics with well- known bulk properties. It belongs to the class of perovskite crystal structures with general formula ABO_3 and has a high-temperature cubic paraelectric state and a low-temperature tetragonal ferroelectric state (Figure 1.4). In bulk $PbTiO_3$, the first order phase transition between these two states takes place around $T_c = 490°C$. In the tetragonal state, the relative z-coordinates of some ions is shifted with respect to the cubic state, which gives rise to a polarization along the [001]-direction. This spontaneous polarization is as high as $P_0 = 0.75C/m^2$ at room temperature, one of the largest spontaneous polarizations of all known ferroelectrics. $PbTiO_3$ displays, as many tetragonal perovskites, a strong polarization-strain coupling, which makes them ideal candidates to modify their properties by (epitaxial) strain. This is generally called "strain engineering". An overview of the most important properties and parameters of lead titanate is given in appendix 6.4.

Because there is a strong relation between the structure and properties of the perovskite ABO_3 compounds discussed here, some more details on their general properties are of interest. The general mechanism[1] for ferroelectricity in ABO_3 perovskites, is a shift of the B-site transition metal cation with a nonmagnetic d^0 electronic structure. In the past sixty years, many of such d^0 perovskite ferroelectric compounds and solid solutions have been studied, a handful of characteristic examples are reported in references [14, 15, 18, 21, 22]. The requirement of "d^0-ness" has been explained in terms of covalent bond formation between empty transition metal d orbitals and filled O $2p$ orbitals [9]. In the case of our "parent compound" $PbTiO_3$, the Pb^{2+} ion has an empty $6p$ orbital, the Ti^{4+} has empty $3d$ and $4s$ orbitals and the O^{2-}'s have

[1] Of course, there are exceptions from this generality. The ferroelectricity in the so-called "geometrical ferroelectric" $YMnO_3$ is driven by MnO_5 polyhedron rotations [20].

filled $2p$ orbitals. Whereas the empty d and filled $2p$ orbital-configurations are of importance for the existence of ferroelectricity, the Pb orbital-configuration is a less strict requirement. As long as the A-ion allows the perovskite phase to stabilize with a d^0 transition metal cation, the material can be ferroelectric. Therefore, in analogy with the charge state of compound semiconductors, 1/5, 2/4 and 3/3 systems can be distinguished. Not only $PbTiO_3$ (2/4), but also compounds like $BaTiO_3$ (2/4), $BiFeO_3$ (3/3) and $KNbO_3$ (1/5) are ferroelectric.

However, the A-cation does play an important role in the ferroelectric behavior and the large spontaneous polarization observed in the pure $PbTiO_3$ compound, compared to other $ATiO_3$ ferroelectric perovskites, has been explained by a strong hybridization between the Pb^{2+} and O^{2-} ions [9]. Despite this large polarization, pure $PbTiO_3$ is not amongst the ferroelectrics most frequently used in commercial applications; $PbTiO_3$-based solid solutions are, instead, utilized. The reason for this is the increase in susceptibilities when the composition is tuned to be in the proximity of the MPB. Solid solutions based on $PbTiO_3$, like PZT, PMN-PT, PSN-PT and PZN-PT[2] have a phase diagram in which many of their susceptibilities like the dielectric constant, $\epsilon(\epsilon_{ij} = \chi_{ij} + 1)$; $\chi_{ij} = (\frac{\delta P_i}{\delta E_j})_T)$, electromechanical coupling constants, k_{ij}, and piezoelectric coefficients, $d_{ij}(d_{ij} = (\frac{\delta P_i}{\delta s_j})_T$; where s is stress), vary as a function of their composition and peak at the MPB between a tetragonal and a rhombohedral phase. It is quite remarkable that solid solutions like PZT, PMN-PT and PZN-PT show enhanced susceptibilities, since these materials are solid solutions of the ferroelectric $PbTiO_3$ and, respectively, the antiferroelectric $PbZrO_3$ and the relaxors $PbMg_{1/3}Nb_{2/3}O_3$ (PMN) and $PbZn_{1/3}Nb_{2/3}O_3$ (PZN)[3]. Analyzing these solid-state solutions as mixtures does not immediately suggest that they should have enhanced susceptibilities. However, one should look at them as an ABO_3 compound with ion replacement on either the A or the B site. Ion replacement is an effective means to change the crystal symmetry and produces non-linear effects in the

[2]These abbreviations are commonly used in the field of ferroelectrics and stand for $PbZr_{1-x}Ti_xO_3$ (PZT; MPB at $x \approx 0.48$), $Pb(Mg_{1/3}Nb_{2/3})_xTi_{1-x}O_3$ (PMN-PT; MPB at $x \approx 0.65$), $Pb(Sc_{1/2}Nb_{1/2})_xTi_{1-x}O_3$ (PSN-PT; MPB at $x \approx 0.60$) and $Pb(Zn_{1/3}Nb_{2/3})_xTi_{1-x}O_3$ (PZN-PT; MPB at $x \approx 0.92$).

[3]Relaxors are ferroelectric materials with a complex behavior. They have cation-disorder between B or A cations with different valences that induces broad frequency-dependent dielectric response.

compounds' dielectric response. Replacement of the Ti^{4+} by the homovalent Zr^{4+} in PZT is a straightforward choice: Only the ion-size changes and this gives rise to so-called "chemical pressure", which will be seen in more detail in the next section. But also replacement by a mixture of heterovalent Sc^{3+} and Nb^{5+} is possible, where $(Sc^{+3}_{1/2}Nb^{+5}_{1/2})^{+4}$ allows relaxor behavior to be displayed. In cases where either the valence or the sizes of the cations differ considerably, they can lead to interesting ordering effects [22].

2.3 Chemical pressure and epitaxial strain

Different models exist to explain the previously described enhancement of dielectric properties. We will treat these models here shortly in the chronological order in which they have been published. A more thorough description can be found in literature [16].

The early work on $PbZr_{1-x}Ti_xO_3$ (PZT) led to the general believe that the MPB in PZT (the first MPB known) around $x \approx 0.50$ is a region of coexistence of tetragonal Ti-rich and rhombohedral Zr-rich phases. During the renaissance of piezoelectricity research in the 1990s, this model was expressed in several papers, most notably by Cao and Cross [14]. They state that the existence of a tetragonal and rhombohedral phase which are equivalent in energy, makes it conceivable that electric-field or stress-driven phase transitions in between these two ferroelectric phases are possible. The increased availability of polar states in the region of coexistence of the two phases, could explain the enhanced dielectric and piezoelectric properties of PZT. Progress in this understanding was hampered by the lack of single crystals of PZT.

In 1997, Park and Shrout [18] observed that in PZN-PT and PMN-PT-crystals close to the MPB, the largest piezoelectric response is along the [001]-direction. This is remarkable because a large response along the [001]-direction is associated with a tetragonal symmetry, while these crystals have a rhombohedral symmetry (with the polar axis along the [111]-direction). Park and Shrout proposed a model based on "domain engineered configurations": At low applied electric fields, the polar vectors in each rhombohedral domain variant will rotate continuously towards the [001]-direction of the applied field. At high electric fields, all polarization rotation ceases and an electric-field induced phase transition to a tetragonal phase will occur with the polar-

ization along the [001]-direction. This implies that at low fields the symmetrically oriented rhombohedral domains effectively produce a macroscopic tetragonal symmetry. At large fields, an electric field-induced phase transition gives rise to phase coexistence and the enhanced properties associated with this transition.

Although these models could explain many aspects of the unusual fer-

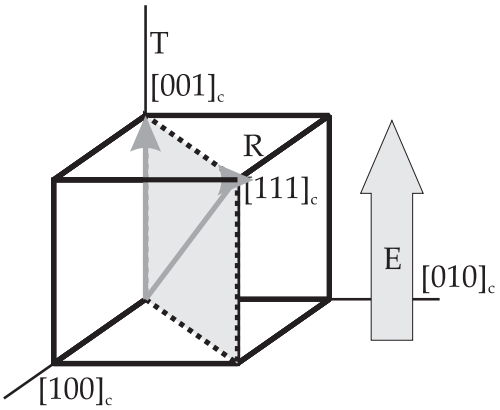

Figure 2.1: Illustration of polarization rotation: an applied electric field E along the [001] direction rotates the polarization from the rhombohedral $[111]_c$-direction towards the tetragonal $[001]_c$-direction. The polar axis of the monoclinic phase is not fixed but is free to rotate within the mirror plane (gray) between the limiting directions of the rhombohedral (R) and tetragonal (T) phases.

roelectric response close to the MPB very well, the rhombohedral-tetragonal phase coexistence was discarded shortly afterwards. Careful analysis of high-resolution synchrotron X-ray powder diffraction revealed an unexpected monoclinic phase at the MPB of PZT [21]. The only symmetry element of this monoclinic phase with space group Cm is a mirror plane; the only common element of the tetragonal $P4mm$ and the rhombohedral $R3m$ phase. Therefore, the monoclinic phase forms, symmetry-wise, a logical connection between the two phases (see Figure 2.1). Somewhat later, the stability of the monoclinic phase close to the MPB with a random Zr/Ti cation distribution was reproduced by first-principles calculations by Bellaiche et al. [23]. Vanderbilt and Cohen [24] predicted by a Landau-Devonshire approach two more "connecting" monoclinic phases between perovskite phases which have been shown to be present experimentally in solid solutions like

PMN-PT [25]. Besides these observations and their theoretical foundation, the monoclinic phase allows for a clear-cut explanation of the enhancement of ferroelectric properties close to the MPB. Fu and Cohen [17] reported first-principles calculations showing the mechanism of polarization rotation: the high electromechanical response in rhombohedral PMN-PT and PZN-PT under an electric field in the [001]-direction, was due to rotation of the polarization in the plane defined by [001] and [111] (Figure 2.1). In the case of Cm compounds, like PZT, this is the monoclinic plane, so the existence of a monoclinic phase close to the MPB allows for polarization rotation and could, therefore, explain the enhanced piezoelectric response [23]. Again, the change in symmetry can be thought to be caused by the "chemical pressure" that the cation replacement of the Ti atom by the somewhat larger Zr atom, brings about.

The difficulty of observing a monoclinic phase by an averaging technique like X-ray diffraction became clear in an article by Khachaturyan, Viehland and collaborators [26] and their idea has been later refined by Wang [27]. They showed that a nanoscale coherent mixture of ferroelectric tetragonal nanodomains can be interpreted as an adaptive ferroelectric phase (similar to those appearing in martensites), whose nanodomain-averaged crystal lattice is monoclinic. Indeed, a size reduction of the domains is expected at the MPB due to the decrease in anisotropy. This complicates the observation of a monoclinic phase and requires measurement techniques probing different length scales to distinguish between an externally driven phase transition, a monoclinic phase or a combination of both. The reason for this is that the average structure and the structure at the unit cell level can be quite different in these ferroelectric solid solutions with intrinsic cation disorder. Based on the observations of Khachaturyan and co-workers, Theismann et al. [28] recently proposed a model in which the enhancement of piezoelectric properties close to the MPB of PZT is extrinsic and closely connected to the existence of tetragonal nanodomains. They showed switching experiments in which mainly the nanodomain structure responds to an electric field. As the number of nanodomains increases upon approaching the MPB and their size decreases, this leads to the thought that the presence and number of nanodomains is related to the enhanced ferroelectric properties close to the MPB.

Treating both intrinsic and extrinsic contributions to piezoelectric properties, Damjanovic [15] stressed the presence of extrinsic effects, but more

importantly proposed an intrinsic model for the enhanced piezoelectric response close to the MPB. Using Landau-Ginzburg-Devonshire thermodynamic theory, Damjanovic showed that the nature of the high piezoelectric response along non-polar directions can be interpreted in terms of the flattening of the Gibbs free energy profile as the composition changes from either end member towards the MPB. He points out that close to any phase transition, flattening of the energy landscape occurs. This automatically gives rise to an increase in dielectric constant, which is inversely proportional to the derivative of the Gibbs free energy, and allows for enhancement of piezoelectric properties, also outside the MPB region. Moreover, a flat energy profile means that the crystal is very susceptible to polarization rotation, both in line with observations. The most common observation of this enhancement of dielectric and piezoelectric responses takes place close to T_c at the ferroelectric-paraelectric phase transition at any composition. But the strong temperature dependence makes these cases much less useful than the enhancements at the MPB, which has very little temperature-dependence.

Since then, many different articles have appeared using different measurement techniques showing either an externally driven phase transition, a monoclinic phase or a combination of both. One important drawback in the interpretation of the experiments and their modeling is the complex chemistry and disordered nature of all materials showing MPBs. One way to overcome this issue is to use the pure $PbTiO_3$ compound and replace the "chemical pressure" by epitaxial strain to induce a MPB. For thin films of $PbTiO_3$ that are sufficiently thin to accommodate the misfit stress with the substrate by unit cell deformation (i.e. lattice strain), epitaxial strain can be used to lower the symmetry to obtain monoclinic-like phases, in line with the model by Noheda et al. [21]. This requires substrates with lattice parameters close to those of $PbTiO_3$, since experiments show that misfit strains larger than $\pm 2\%$ cannot be accommodated by lattice deformation [29]. Knowing the temperature dependence of the lattice parameters of $PbTiO_3$ (Figure 1.5), this means that substrate lattice parameters between 3.827 and 3.983 Å at room temperature are required.

On the other hand, partially strained thin films can be obtained when the thicknesses are slightly above the critical thickness for strain relaxation. These put less stringent measures on the substrate lattice parameters and generally show nanoscale domains. Therefore, these films can be used to

verify the role of nanodomains [26, 28] either in defining the macroscopic symmetry of the materials showing large piezoelectric response or in determining the role of domain walls on the piezoelectric response. In conclusion, for all models, epitaxial strain in ferroelectric thin films could be an effective means to investigate and modify the piezoelectric response. Whereas the presence of a monoclinic phase can be tested in strained thin films with a modified crystal structure, the presence of nanodomains with densities varying with thickness can help understanding the role of domain walls on the dielectric and piezoelectric properties. Thin films of pure $PbTiO_3$ can help elucidate the applicability of either of the two models and in combination with reliable measurement of the ferroelectric properties of these (ultra)thin films, this allows to show the importance of the presence of the monoclinic phase or nanodomains. Unfortunately, reliable measurement of the ferroelectric properties of these (ultra)thin films remains problematic and resolution of nanodomains by standard diffraction techniques is not possible.

2.4 Bulk ferroelectric perovskites

We will now discuss the two pathways generally used to model ferroelectrics like $PbTiO_3$. On the one hand, a theoretical microscopic view is used in which the ferroelectric is described by a Hamiltonian with parameters obtained by first principles. On the other hand, a macroscopic view based on experimental observations, allows to use the Landau(-Ginzburg-Devonshire, LGD) approach in which the Gibbs Free Energy with experimentally obtained parameters is the starting point of the description (phenomenology). Both approaches will be briefly described here, centered around seminal works on $PbTiO_3$ by Cohen [9], Bellaiche [23], Waghmare and Rabe [30] and Meyer and Vanderbilt [31](first principles) and Landau [32] and Pertsev [33] (phenomenology).

2.4.1 First principles

The atomic structure and interatomic interactions of displacive perovskite ferroelectrics are central to their theoretical description. As already pointed

out in section 2.2, Cohen [9] has been able to explain the existence of ferroelectricity in the classical ferroelectrics $PbTiO_3$ and $BaTiO_3$ very well by using first-principles electronic-structure calculations. He showed that in these materials, hybridization between the titanium $3d$ and oxygen $2p$ states is essential for ferroelectricity. More complex systems of disordered solid solution have been successfully described by Bellaiche et al. [23]. They have been the first ones to reproduce the monoclinic phase in PZT by first principles calculations. The core of many first-principles calculations is formed by the ultrasoft pseudopotentials as described by Vanderbilt in 1990 [34]. These potentials can describe the total-energy surface of perovskites, predicting materials' characteristics like the crystal symmetry, lattice parameters, elastic constants and band structures.
A different approach was employed by Waghmare and Rabe [30] who constructed a first-principles effective Hamiltonian model through the use of a localized, symmetrized basis set of "lattice Wannier functions" which mathematically shows strong resemblance with phenomenological Landau expansions [35]. Their model Hamiltonian is based on lattice dynamics and is essentially a function of the unstable phonons of the high-symmetry reference structure, i.e. the soft-mode distortion ξ. Explicitly, their Hamiltonian reads:

$$H_{mod}^{bulk}(\xi) = A\xi^2 + B\xi^4 + C\xi^6 + D\xi^8 \tag{2.1}$$

Since the soft-mode distortion is an order parameter of the ferroelectric transition, the similarities with the Landau expansion in the next paragraph are easily seen. Indeed, the definition of polarization from a microscopic point of view, easily shows this relation between the polarization $\mathbf{P}$ and the average uniform local distortion $\langle\xi\rangle$:

$$\mathbf{P} = \frac{\mathbf{Z}^* . \langle\xi\rangle}{V_{cell}} \tag{2.2}$$

Where $\mathbf{Z}^*$ is the mode effective charge and V_{cell} the unit-cell volume. This describes the mechanism very well and allows to extract the symmetry of the ferroelectric phase through the symmetry of the soft-mode. For ferroelectric thin films, the comparison of experiment and theory may be difficult because the measurement of both the polarization and the atomic positions is very challenging. Fortunately, Landau theory provides insight into coupling

between the polarization and an easier accessible measurement: the tetragonality c/a.

2.4.2 Phenomenology

The phenomenological Landau theory [32] solely uses symmetry considerations, to describe a system's equilibrium behavior near a phase transition. It is a strictly macroscopic approach, expressing the free energy as a power series expansion of an order parameter of the phase transition. The input coefficients for this free energy expression can be obtained experimentally or via first-principles approaches, but the experimental ones are most often used.

Several considerations are needed to apply this theory: The order parameter should be small (i.e. this does not hold far from T_c or for strongly first order transitions) and a good knowledge of the symmetry of the phases on opposite sides of the phase transition is required. For the paraelectric-to-ferroelectric transition, one macroscopic order parameter is the polarization $\mathbf{P}(T)$. The Gibbs free energy, G, is the most appropriate energy expression (the stress is not a function of the polarization) and it can be expressed as a function of the main order parameter, $\mathbf{P}$, the electric field, $\mathbf{E}$, and the strain, u. While it is, in principle, not correct to use the Helmholtz free energy (it allows for non-constant pressure), this is often done since it can be expressed as a function of an experimentally convenient parameter: strain, u (whereas Gibbs free energy is expressed in terms of stress). The Gibbs free energy at zero field and pressure with a power series expansion of $\mathbf{P}$ should only contain symmetry-allowed elements ($m3m$ for $PbTiO_3$), thus $G(\mathbf{P}) = G(-\mathbf{P})$. In the case of perovskites with a cubic parent phase, the symmetry-allowed power series (up to 6th order) of the main order parameter $\mathbf{P}$ plus the electric field $\mathbf{E}$ and temperature T-dependence give:

$$G(\mathbf{P}, \mathbf{E}, T) = -\mathbf{E}\mathbf{P} + G_o + c_2(T)\mathbf{P}^2 + c_4\mathbf{P}^4 + c_6\mathbf{P}^6 \tag{2.3}$$

where c_6 has to be larger than zero to obtain stable states. All c_i coefficients could in principle depend on temperature, but it is shown that the phase transitions can be well reproduced by considering that all the dependence on temperature is contained in c_2. If c_2 is expanded in a series of T around the Curie temperature Θ (which is equal to or less than the phase transition

temperature T_c), until first order, we get

$$c_2 = \frac{1}{C}(T - \Theta) \tag{2.4}$$

And the stable states can be obtained by solving

$$\frac{\delta G}{\delta \mathbf{P}} = -\mathbf{E} + \mathbf{P}(c_2 + c_4\mathbf{P}^2 + c_6\mathbf{P}^4) = 0 \tag{2.5}$$

and

$$\frac{\delta^2 G}{\delta \mathbf{P}^2} = \frac{1}{\chi} = c_2 + 3c_4\mathbf{P} + 5c_6\mathbf{P}^3) > 0 \tag{2.6}$$

The case with $c_4 > 0$ corresponds to a second order phase transition. Then c_6 is not needed to provide stable states and we can consider c_6=0 as a first approximation (see figure 2.2). But bulk $PbTiO_3$ displays a first-order transition, which means that $c_4 < 0$ and thus $c_6 > 0$. The paraelectric phase corresponds to the trivial solution $\mathbf{P} = 0$. Combining equations 2.4 and 2.6 and bearing in mind that c_2 contains the temperature-dependence, it can be shown that the dielectric susceptibility, χ, follows a Curie-Weiss law:

$$\chi = \frac{C}{T - \Theta} \tag{2.7}$$

This approach can be expanded by introducing, besides spontaneous polarization, also spontaneous strain and by considering their vectorial and tensorial characters, respectively. This results in the power series expansion of the free elastic Gibbs energy functional as proposed by Haun et al. [13]. Generally, four different solutions to these Landau equations exist, corresponding to the different symmetries of perovskite ferroelectrics with different polarization directions (see Figure 2.3):

Cubic	$P_1 = P_2 = P_3 = 0;$
Tetragonal	$P_1 = P_2 = 0, P_3 \neq 0;$
Orthorhombic	$P_1 = P_2 \neq 0, P_3 = 0;$
Rhombohedral	$P_1 = P_2 = P_3 \neq 0$

where (P_1, P_2, P_3) are the cartesian components of the polarization vector, $\mathbf{P}$. In the case of bulk $PbTiO_3$, only the first two phases are of importance,

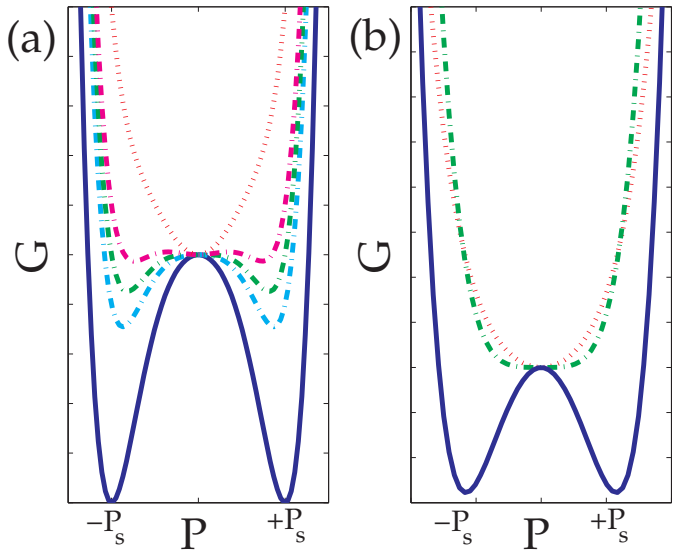

Figure 2.2: Gibbs free energy of a ferroelectric with (a) a first-order phase transition (c_4 <0 and c_6 >0) and (b) with a second-order phase transition (c_4 >0 and c_6 =0) at different temperatures. The solid line corresponds to T< T_c (ferroelectric, c_2 <0), the dash-dotted line to T= T_c (c_2 =0) and the dotted line to T> T_c (paraelectric, c_2 >0). In the case of a first-order transition, the cases just below and above T_c are also plotted.

since the latter two are not observed. Recent work by Vanderbilt and Cohen [36] has shown that expansion of the free energy to 8th order can give rise to monoclinic phases and that 12th order expansion is required to obtain triclinic ferroelectric phases, with these polarization directions:

$$\begin{array}{ll} \text{Monoclinic} & P_1 = P_2 \neq 0; P_3 \neq 0; P_1 \neq P_3; \\ \text{Triclinic} & P_1 \neq 0; P_2 \neq 0; P_3 \neq 0; P_1 \neq P_2 \neq P_3; \end{array}$$

Orthorhombic and rhombohedral phases can be observed in many well-known ferroelectrics, such as $BiTiO_3$. Lower symmetry phases have only been observed so far in MPB systems [18, 21, 25]. However, Pertsev [33] has shown that these latter phases can be observed in $PbTiO_3$ thin films, as we will discuss in the next section. For the bulk phases of $PbTiO_3$, the characteristic pa-

rameters, as listed in the appendix, have been determined by Haun et al. [13] by measuring the critical temperatures, Curie constants and zero-field polarization. In the next sections we will use these characteristic coefficients to determine the phases and energy expressions of thin films of $PbTiO_3$.

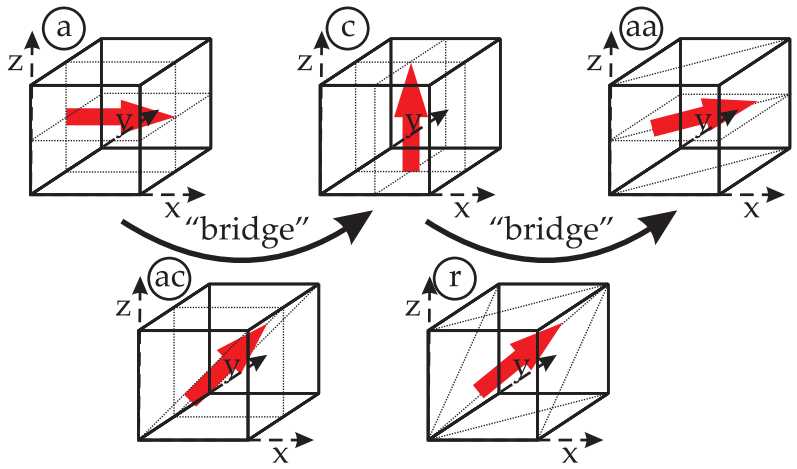

Figure 2.3: Polar axes of the different crystallographic phases of monodomain epitaxial $PbTiO_3$ thin films. The "bridging" indication shows the most likely locations of the ac and r phases in the phase diagram in Figure 2.4 and 2.5.

2.5 Thin films of ferroelectric perovskites

The geometry usually considered for the study of ferroelectric thin films is that of an infinite single-crystalline planar slab clamped to a substrate. In this geometry, two thermodynamic variables should be considered which determine the properties of ferroelectric thin films. First of all, the stress field (due to the mechanical boundary conditions imposed by the substrate) and second the electric field (i.e. the electrical boundary conditions due to the presence or absence of electrodes). Both variables can, in principle, be eliminated. The electric field can be eliminated by shortening top and bottom electrodes. More troublesome is the elimination of the stress field which can be done by

making a free-standing thin film [4]. In most experimental setups, both stress and electric field are present and play an important role.

2.5.1 Ultrathin films

The main focus of first principles calculations on thin films, is on ultrathin films. The limited size of ultrathin films enables the atomistic simulation over their entire thickness. Studies have clearly shown that the critical thickness for ferroelectricity depends on the mechanical and electrical boundary conditions. Although Meyer and Vanderbilt have suggested the absence of a fundamental critical thickness for ferroelectricity in ideal short-circuited films [37], most reports on realistic systems show critical thicknesses of the order of several unit cells which critically depends on the electrodes. Junquera and Ghosez [38] have shown, for example, a critical thickness of six unit cells for $BaTiO_3$ with symmetric $SrRuO_3$ electrodes. They point out that a depolarizing electrostatic field, caused by dipoles at the ferroelectric/metal interfaces, is the reason for the disappearance of the ferroelectric instability. Experimentally, Fong et al. [1] have shown that thin films of $PbTiO_3$ on insulating $SrTiO_3$ substrates are ferroelectric down to 3 unit cells. In addition, the group of Triscone has shown that the tetragonality of ultrathin $PbTiO_3$ films decreases with decreasing film thickness [39]. And even more importantly for the work described in this thesis, they have shown that the electrical boundary conditions play a key role on the ferroelectricity and the ferroelectric domain structure of very thin $PbTiO_3$ films.

2.5.2 Phenomenology of thin films

Phenomenological models of monodomain thin films, like that of Pertsev et al. [33], are based on the previously described Landau expansion as proposed by Haun et al. [13]. It is assumed that the ground state of the grown film is cubic paraelectric and the mechanical boundary conditions posed by the substrate on the thin film have been added to describe the strain effect on

[4] For the typical film thickness we used, this implies etching the substrate while leaving the thin film intact, which is very challenging and time-consuming.

monodomain ferroelectric thin films:

$$\begin{aligned}\widetilde{G} = {} & \alpha_1^*(P_1^2+P_2^2)+\alpha_3^*P_3^2+\alpha_{11}^*(P_1^4+P_2^4)+\alpha_{33}^*P_3^4 \\ & +\alpha_{13}^*(P_1^2P_3^2+P_2^2P_3^2)+\alpha_{12}^*P_1^2P_2^2+\alpha_{111}(P_1^6+P_2^6+P_3^6) \\ & +\alpha_{112}\left[P_1^4(P_2^2+P_3^2)+P_3^4(P_1^2+P_2^2)+P_2^4(P_1^2+P_3^2)\right] \\ & +\alpha_{123}P_1^2P_2^2P_3^2+\frac{u_m}{s_{11}+s_{12}}\end{aligned} \tag{2.8}$$

This lengthy Landau expression up to the 6^{th} order term in the polarization includes parameters modified by strain effects (hence the asterisks) and temperature and the last term also accounts for the misfit strain, u_m. This expression is used to obtain phase diagrams as shown in Figure 2.4 and 2.5.

It is important to know how the misfit strain u_m is defined, because different definitions of it are used in the literature. By experimentalists, the misfit strain in a substrate/thin film system is defined as the difference in in-plane bulk lattice parameters between substrate and film, normalized by the substrate lattice parameter. Using the room temperature lattice parameters of bulk $PbTiO_3$ (a=3.905 Å) and one of the substrates used in this thesis work, $DyScO_3(110)_o$ (b=3.948 Å, approximately, since $DyScO_3(110)_o$ does not have a perfect cubic in-plane lattice [40]), this gives a misfit strain

$$u_{m,tet} = \frac{b-a}{b} = \frac{3.948\mathring{A} - 3.905\mathring{A}}{3.948\mathring{A}} = +0.011 \tag{2.9}$$

Where b is the in-plane substrate lattice parameter, a is the bulk in-plane thin film lattice parameter and the subscript tet stands for the fact that the misfit is calculated for tetragonal $PbTiO_3$. This definition differs considerably from that used by theorists. For a theoretical description of ferroelectrics like $PbTiO_3$, the material is assumed to be "self-strained": the ground state of the material under zero stress is thought to be cubic paraelectric state and the (tetragonal) ferroelectric state is described as a deformation from the cubic phase by a self-strain. For $PbTiO_3$ (see Appendix 6.4), this means that, at room temperature, the self-strained bulk lattice has lattice constants a=3.905 Å and c=4.156 Å [41], whereas the pseudocubic lattice without self-strain has a lattice constant a_0=3.961 Å, as obtained from an extrapolation of the experimental cubic lattice parameters to low temperatures [13]. This means that the

misfit strain at room temperature is defined as

$$u_{m,cub} = \frac{b - a_0}{b} = \frac{3.948\mathring{A} - 3.961\mathring{A}}{3.948\mathring{A}} = -0.0033 \tag{2.10}$$

This implies that, whereas some would state that at room temperature c-oriented $PbTiO_3$ on $DyScO_3(110)_o$ has a $+1.1\%$ tensile misfit, others would state that the misfit is compressive and only -0.33%. This means a change in sign of the misfit, combined with a difference of a factor ~ 4. Especially in the specific cases treated in this thesis, these differences in definition can be very confusing: some would say $PbTiO_3$ on $SrTiO_3$ has a small misfit strain at room temperature compared to $PbTiO_3$ on $DyScO_3$, while others would state exactly the opposite. For this reason, the words "small" and "large" in the titles of the next chapters are within quotes. Throughout this thesis, we will always mention which definition of the misfit strain is being used.

Back to Pertsev's model [33], the most important observations from Figure 2.4 are the change of the order of the paraelectric/ferroelectric phase transition, which changes from first to second order for $PbTiO_3$ and the huge shift of T_c with strain, with respect to the bulk values. This can be explained by the change in the α-constants. For instance, for the paraelectric to c phase transition, from α_{33} to α^*_{33} constant: the former equals $-7.3 \times 10^7 \frac{m^5}{FC^2} < 0$ and thus corresponds to a first order phase transition whereas the latter equals $\alpha_{33} + \frac{Q_{12}^2}{s_{11}+s_{12}} = +5.0 \times 10^7 \frac{m^5}{FC^2} > 0$ which corresponds to a second order phase transition. Besides, the critical temperature T_c is shifted upwards. The shifted temperature is described for the paraelectric-to-aa phase transition ($u_m \geq 0$) by

$$T_c = T_0 + 2C\epsilon_0 \frac{Q_{11} + Q_{12}}{s_{11} + s_{12}} u_m \tag{2.11}$$

and, for the paraelectric-to-c phase transition ($u_m \leq 0$) by

$$T_c = T_0 + 2C\epsilon_0 \frac{2Q_{12}}{s_{11} + s_{12}} u_m \tag{2.12}$$

where Q_{ij}'s are the electrostrictive coefficients, s_{ij}'s are the elastic compliances at constant polarization, C is the Curie-Weiss constant and ϵ_0 is the dielectric susceptibility of vacuum. Assuming a maximum misfit of 2%, the T_c can be shifted as much as 600°C upwards.

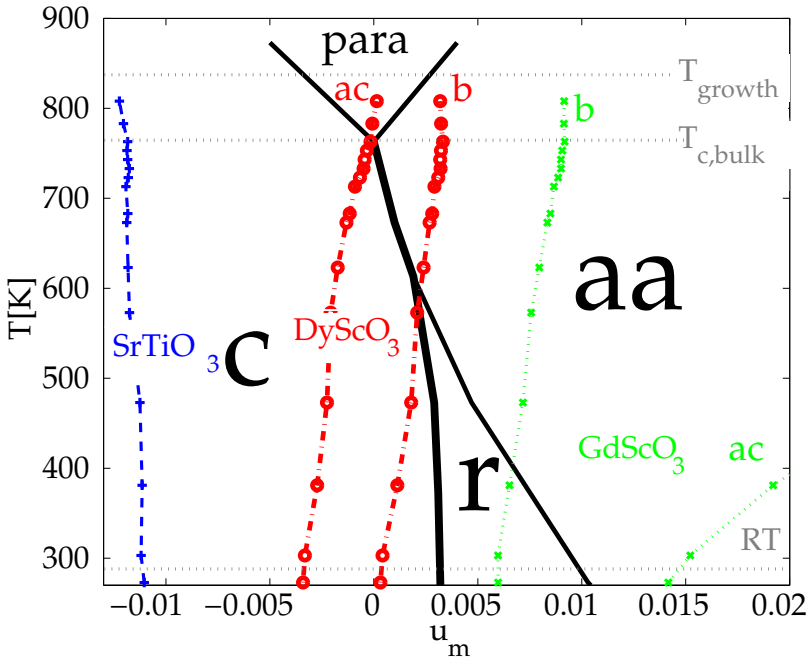

Figure 2.4: u_m-T phase diagram and some combinations of $PbTiO_3$ on (pseudo)cubic substrates providing various misfit strains u_m(T) curves. The triple point at u_m=0 corresponds to the Curie-Weiss temperature of bulk $PbTiO_3$. The circles correspond to $DyScO_3(110)_o$ substrates, the squares to $GdScO_3(110)_o$ and the crosses to $SrTiO_3(001)_c$. The first- and second-order phase transitions are shown by thick and thin lines, respectively. "Para" stands for the paraelectric phase and the bulk T_c, the growth temperature and room temperature are also indicated. This figure is constructed using the phase diagram from the articles by Pertsev et al. [33] and the lattice parameters from Shirane et al. [10] and Biegalski et al. [40].

Finally, at low temperatures, the clamping to the substrate can stabilize the aa phase (orthorhombic) and the r phase (monoclinic) with two and three nonzero components of the polarization. These phases do not exist in free bulk $PbTiO_3$ crystals. It is worth to notice that the substrate lattice parameters have to fulfill very strict conditions in order to obtain these phases experimentally [42]. The r-phase only exists for temperatures below T≈320°C on substrates with in-plane lattice parameters above 3.968 Å at this temperature

(∼3.949 Å at room temperature). Combined with the maximum misfit strain which can be accommodated by lattice deformation (∼2%; section 2.3), this leads to the conclusion that the room temperature c-phase of $PbTiO_3$ requires effective substrate lattice parameters between 3.827 and 3.949 Å and for the r-phase they should be between 3.949 and 3.983 Å.

The more elaborate case of anisotropic in-plane strain, applicable when

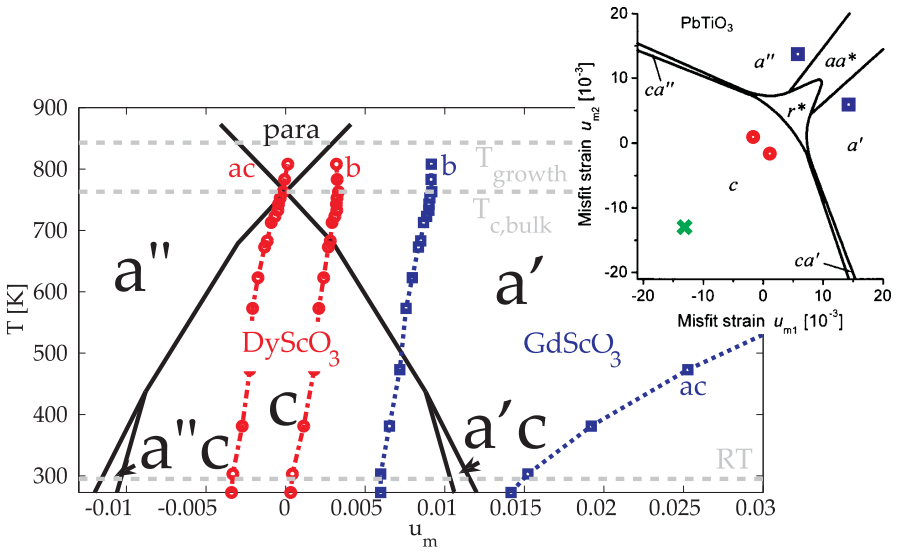

Figure 2.5: Vertical cross section of the three-dimensional phase diagram of $PbTiO_3$ thin films grown on dissimilar orthorhombic substrates. This cross section corresponds to the plane u_{m1}=-u_{m2}. The circles correspond to $DyScO_3(110)_o$ substrates, the squares to $GdScO_3(110)_o$ and the green cross to $SrTiO_3(001)_c$. The single(′) and double(″) prime correspond to the two distinctive a-directions, for which the polarization is oriented along the [100] and [010] crystallographic axes, respectively. Indicated are also the bulk T_c, the growth temperature and room temperature. The inset shows a horizontal cross section of this three-dimensional phase diagram at $T = 25°C$. This figure has been constructed using the phase diagrams from articles by Zembilgotov et al. [43] and the lattice parameters from Shirane et al. [10] and Biegalski et al. [40].

substrates with an in-plane rectangular structure are used, has been analyzed by Zembilgotov et al. [43]. The misfit strain, u_m, is replaced by two misfit strains, u_{m1} and u_{m2}, for the two different in-plane directions. This extra pa-

rameter gives rise to a three-dimensional phase diagram of which the most interesting profiles are reproduced in Figure 2.5. The inset of this figure displays the profile of the $u_{m1}, -u_{m2}$ plane at room temperature and shows that, in the case of anisotropic strain, the requirements on the substrate parameters in order to obtain the r-phase, are somewhat relaxed. A tensile lattice misfit is required and lattice parameters between 3.949 Å and 4.000 Å are necessary.

Finally, note that it is quite surprising that this theory works well to describe ferroelectric $PbTiO_3$, since the primary requirements are not very well met: the cubic-to-tetragonal phase transition in bulk $PbTiO_3$ is strongly first order and room temperature is relatively far from $T_c = 490°C$. In thin films under strain, the phase transition changes from first to second-order [33] which improves the suitability of the theory, but T_c is shifted upwards under the influence of stress, which makes it more remarkable that the theory describes thin films at room temperature under epitaxial strain (stress) quite well.

2.5.3 Tetragonality

Besides the previously described phase diagrams, Landau models can also be used to gain more insight in the relationships between different physical properties. In the case of a thin film, the normal stress σ_3 is always zero which enables the calculation of the u_3 strain tensor [13] via the thermodynamic relation $\sigma_3 = \frac{\delta G}{\delta u_3}$ and the Gibbs free energy as described by Haun et al. [13]:

$$\frac{\delta G}{\delta u_3} = 0 = C_{11}u_3 + 2C_{12}u_1 - Q_{11}P_3^2 \tag{2.13}$$

where Q_{ij} are the cubic electrostrictive coefficients and C_{ij} the second order elastic coefficients, which can be rewritten as

$$u_3 = \frac{1}{C_{11}}(Q_{11}P_3^2 - 2C_{12}u_1) \tag{2.14}$$

By using the definition of strain:

$$u_3 = \frac{c-a}{a} \Rightarrow c = a(1+u_3) \tag{2.15}$$

and rewriting this, one can get the tetragonality of an epitaxial film, which can be measured:

$$\frac{c}{a_{sub}} = \frac{a}{a_{sub}}(1 + u_3) \tag{2.16}$$

We can combine equation 2.14 and 2.16 to obtain

$$\frac{c}{a_{sub}} = \frac{a}{a_{sub}}(1 + \frac{1}{C_{11}}(Q_{11}P_3^2 - 2C_{12}u_1)) \tag{2.17}$$

This shows that for constant u_1, the tetragonality (c/a) of a [001]-oriented strained film scales with P_3^2. This coupling will be used throughout this thesis to monitor ferroelectricity. Temperature dependent measurements of the tetragonality, allow us to probe the order parameter as a function of temperature.

Regarding thickness dependent measurements of the tetragonality, the validity of this relationship is still under debate, certainly for $PbTiO_3$. Whereas several reports show a strong polarization-strain coupling [29, 35], C.-L. Jia et al. [44], have shown that this mechanism is not universal and Lee et al. [45] have shown that it is especially not valid for $PbTiO_3$-based ferroelectrics. It is thought that the already large lattice distortions (and thus polarizations) in the bulk, can not be enlarged by applying additional strain. This would make these materials rather insensitive to applied epitaxial strain above a certain strain regime.

In order to verify the polarization-strain coupling, pure $PbTiO_3$ on different substrates has been used, but the low critical thickness for strain relaxation often hinders verification. Based on the work of Speck and collaborators [46], these critical thicknesses for $PbTiO_3$ on Pt(140 Å) and $SrTiO_3$(83 Å) should be still reasonably large to perform electrical measurements without being dominated by tunneling and leakage currents and interface effects. But as soon as misfits increase, the small critical thicknesses prevent experimentalists from measuring polarization directly (e.g. on MgO the critical thickness is only 5 Å). Therefore, many indirect measurements of polarization by measuring strain, will be influenced by the type of strain relaxation and domain formation. Still, strain is used as an indirect measurement of the large ferroelectric responses, since it is strongly coupled to the symmetry change related to the large ferroelectric responses close to the morphotropic phase boundaries.

2.6 Domain structures in ferroelectric perovskites

In a real thin film, the single-crystalline planar slab described in the previous section, will often show regions with different orientations of the polarization (domains). In a tetragonal ferroelectric perovskite like $PbTiO_3$, two kinds of domains can be distinguished: so-called 180° and 90° domains. The driving forces for their appearance are, respectively, electrostatic and mechanical in origin, as explained in chapter 1. For both types of domains, a critical thickness exists above which the domains and the walls separating them, will appear. For $PbTiO_3$, the critical thickness for 180° domain formation, which do not contribute to the elastic energy, is typically in the order of a few monolayers and close to the critical thickness for ferroelectricity. Whereas the critical thickness for 90° domain formation (strain relaxation) depends heavily on the misfit strain. Above the latter critical thickness, 90° domains form which add complexity to the description of ferroelectric structures. But from the application point of view it is important to take domains into account, because domains play an important role in switching behavior. Extrinsic effects, such as domain wall motion, can even account for more than 50% of the total materials' response in some cases [15].

Regarding the analytical analysis of domains, first-principles calculations on 180° domain structures are most challenging because of the scarcity of atomic scale details on these domain walls [44]. Several characteristic domain wall properties have anyhow been obtained by first-principles calculations. We will elaborate here on the results by Meyer and Vanderbilt [31] and Kornev et al. [47]. Meyer and Vanderbilt have given more details on the energetics of 180° and 90° domain walls and Kornev on the possibilities of rather exotic domain patterns. Next, several phenomenological models will be described, applicable to 180° domains [48], the onset of 90° domains [2, 3] and 90° domain structures [49, 5].

2.6.1 180° domains

Meyer and Vanderbilt [31] have used first-principles in order to calculate the equilibrium structural parameters, the domain wall energies, the atomistic domain-wall structure, the barrier for domain wall motion and the polarization profile of $PbTiO_3$ for both 90° and 180° domain walls. Their main results are summarized in Table 2.1. Note that this analysis is valid for a tempera-

parameter [units]	180° domain walls	90° domain walls
$E_{formation}[mJ/m^2]$	132 (γ)	35 (σ)
$E_{barrier}[mJ/m^2]$	37	1.6

Table 2.1: First principles results by Meyer and Vanderbilt [31] on 90° and 180° domain walls in a free-standing $PbTiO_3$ single crystal. Note that we will use the symbol σ for the 90° domain wall formation energy and γ for the 180° domain wall formation energy.

ture of 0K and a free standing $PbTiO_3$ single crystal. The main observation in these data is that both the domain wall formation energy and the energy barrier for domain wall motion for 90° domains are much lower than those for 180° domains. The energy barrier for 90° domain wall motion ($1.6mJ/m^2$) is of the order of k_BT at room temperature, meaning that 90° domain walls are expected to be still mobile at room temperature. Whereas the energy barrier for 180° domain wall motion is much higher, indicating that 180° domains will instead "freeze in" at an elevated temperature [50].

Kornev et al. [47] have used a first-principles derived effective Hamiltonian to describe the effect of different electrical boundary conditions on polarization patterns in tetragonal PZT close to the MPB. Based on a parameter, β, which describes the total electric field inside the film, they have shown the correlation between the amount of screening of surface charges and the polarization patterns. These correlations differ for different mechanical boundary conditions. Compared to the stress-free situation, in-plane polarization is favored under tensile strain and any in-plane polarization is annihilated for all β values under compressive strain. Under compressive strain, open circuit conditions result in a macroscopically non-polar state (MNP; Figure 2.6c). Increasing β towards short-circuit conditions, gives rise to a microscopically inhomogeneous (Figure 2.6b) and a microscopically homogeneous (Figure 2.6a) polar state, consecutively. The inhomogeneous polar state consists of nanodomains having local dipoles aligned opposite to the macroscopic polarization. The MNP state shows a polarization structure as depicted in Figure 2.6c, which is different from the commonly accepted pictures of out-of-plane 180° flux-closure domains and open-stripe domains [51]. The nanodomain structure reflects the competition between electrical and mechanical bound-

ary conditions. Each nanodomain is terminated at one surface by significant in-plane and relatively small out-of-plane polarizations (1; to decrease the depolarizing field) and has a neighboring nanodomain that is terminated at this surface by rather large out-of-plane polarizations (2; driven by the compressive strain).

The general phenomenological description of 180° domains originates

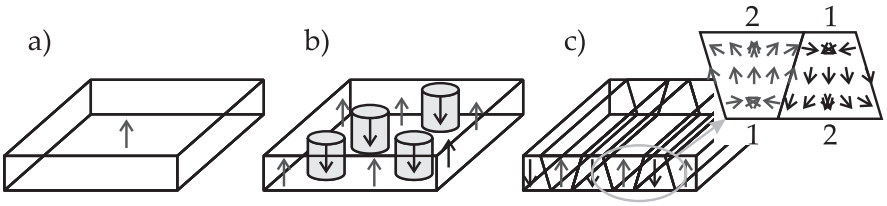

Figure 2.6: Sketch of the three different domain structures presented by Kornev et al. [47]: a) microscopically homogeneous polar state, b) microscopically inhomogeneous polar state and c) macroscopically non-polar state (MNP). The inset of figure c) shows the polarization structure in more detail.

from ferromagnets [51] and has been applied to ferroelectrics too [48]. As previously mentioned, ferromagnets show two types of 180° domains: flux-closure domains and open-stripe domains [51]. Whereas in free-standing ferromagnets, domain formation is determined by a competition between the magnetic field energy, domain wall formation energy and anisotropy energy of spin orientations, in ferroelectrics, the last term does not play any role and the first term naturally involves the electric instead of the magnetic field energy, leading to the formation of only open-stripe domains. For ferromagnets, the flux-closure domains correspond to a non-zero domain wall energy and anisotropy term and a zero magnetic field energy, whereas in a ferroelectric, the analogous case would correspond to zero electrostatic energy and therefore, no domains are formed.

The first comparison between the energy of different domain structures dates back to Lev Landau [32] and Charles Kittel [51], who derived what is now called "Kittel's Law". This law holds for domain systems in which the domain wall energy per unit film surface scales with $\frac{H}{d}$ (thickness/domain width ratio) and the magnetic or electrostatic energy per unit film surface area, scales with the domain width d [52]. Adding these terms and setting

the derivative with respect to d equal to zero[5], gives:

$$c_1 - c_2 \frac{H}{d^2} = 0 \tag{2.18}$$

This means that the energy is minimized for domain sizes that scale with the film thickness according to

$$d \sim \sqrt{H} \tag{2.19}$$

Additional energy terms can modify this situation, which is the case for epitaxial instead of free-standing thin films with 90° domain walls. For ferroelectrics, depending on the leading term in the energy balance, 180° (electrostatic) domains or 90° (elastic) domains will appear. In the remaining of this section, we will give energy expressions of the general form of the energy $F_{total} = F_{wall} + F_{elec} + F_{elas}$ that describes these domain structures.

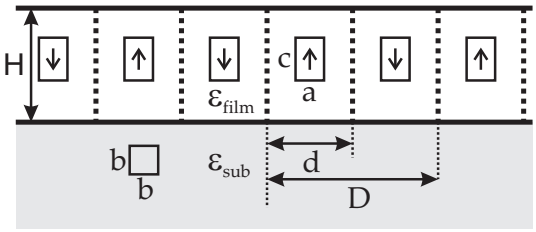

Figure 2.7: Schematic representation of the side-view of a 180° domain pattern, analyzed with and without taking the presence and dielectric constant of the substrate (gray) into account.

Mitsui and Furuichi [48] have derived the ferroelectric analog of Kittel's law that gives an equivalent relationship between the ferroelectric crystal thickness, H, and the 180° domain width, d, in the case that electrostatics is dominant (see Figure 2.7). For a fully relaxed free-standing crystal with 180° domains, the dielectric constant, ϵ, spontaneous polarization, P_0, and

[5]Generally, we will use the domain periodicity D instead of the domain width d. For 180° domains, $2d = D$, but for 90° domains this relation usually does not hold.

the 180° domain wall energy, γ, are also involved in these expressions [48]:

$$\begin{aligned} F_{wall} &= \frac{\gamma(T)H}{D} \\ F_{elec} &= \frac{1.052 \cdot 8 \cdot P_0^2 D}{\pi^3 \epsilon_0 (1+\sqrt{\epsilon_a \epsilon_c})} \\ F_{elas} &= 0 \end{aligned} \tag{2.20}$$

$$F_{total} = \frac{\gamma(T)H}{D} + \frac{1.052 \cdot 8 \cdot P_0^2 D}{\pi^3 \epsilon_0 (1+\sqrt{\epsilon_a \epsilon_c})} \tag{2.21}$$

which can be used to calculate the domain width as a function of the crystal thickness:

$$\frac{\partial F}{\partial D} = -\frac{\gamma(T)H}{D^2} + \frac{1.052 \cdot 8 \cdot P_0^2}{\pi^3 \epsilon_0 (1+\sqrt{\epsilon_a \epsilon_c})} = 0 \tag{2.22}$$

$$D^2 = \gamma(T) H \frac{\pi^3 \epsilon_0 (1+\sqrt{\epsilon_a \epsilon_c})}{1.052 \cdot 8 \cdot P_0^2} \tag{2.23}$$

Mitsui and Furuichi [48] have obtained also several other important properties of 180° domain walls. For the current work, their main results are the relations between the spontaneous polarization, P_0, and both the domain wall width, δ, and the 180° domain wall energy ,γ:

$$\delta = \frac{c'}{P_0} \tag{2.24}$$

$$\gamma = c \cdot P_0^3 \tag{2.25}$$

Equation 2.24 and especially the constant c' has been extracted for many ferroelectrics to show the narrow domain wall width, usually in the order of tens of Ångströms. This is an important observation that justifies the simplification in all models to set $\delta = 0$. Equation 2.25 is very useful when domain wall energies are to be determined, since the temperature-dependence of the polarization is usually well-known. Streiffer et al. [53] have used this relationship and we will apply it similarly here. Domain wall energies calculated by first-principles, like those of Meyer and Vanderbilt [31], hold at $T = 0K$. Since the domain wall energy is proportional to P_0^3, the temperature depen-

dence of the domain wall energy is given by

$$\gamma(T) = \gamma(0K) \left[\frac{P_0(T)}{P_0(0K)} \right]^3 \tag{2.26}$$

Several authors [53, 54, 52] have refined the model of Mitsui and Furuichi by taking the boundary conditions of a dielectric substrate into account. This is of importance because the higher the dielectric constant of the substrate, the better the screening of the depolarization field. Therefore, this external dielectric constant reduces the driving force for the formation of 180° domains and will, in general, lead to larger domain sizes. For a fully relaxed system with 180° domains on a substrate we get:

$$F_{elec} = \frac{1.052 \cdot 8 \cdot P_0^2 D}{\pi^6 \epsilon_0 \epsilon_{sub} (1 + \frac{\sqrt{\epsilon_a \epsilon_c}}{\epsilon_{sub}})} \tag{2.27}$$

$$F_{total} = \frac{\gamma(T) H}{D} + \frac{1.052 \cdot 8 \cdot P_0^2 D}{\pi^6 \epsilon_0 \epsilon_{sub} (1 + \frac{\sqrt{\epsilon_a \epsilon_c}}{\epsilon_{sub}})} \tag{2.28}$$

Which can be minimized with respect to the domain width, resulting in:

$$D^2 = \gamma(T) H \frac{\pi^6 \epsilon_0 \epsilon_{sub} (1 + \frac{\sqrt{\epsilon_a \epsilon_c}}{\epsilon_{sub}})}{1.052 \cdot 8 \cdot P_0^2} \tag{2.29}$$

2.6.2 Critical thickness for strain relaxation

The formation of 180° domains requires single crystallographic orientation. Above the critical thickness for strain relaxation, crystallographic 90° domains form and electrostatics will play a minor role. The thickness at which these domains start to form can be calculated by comparing the free energies of a strained and a relaxed system. This mechanism is an alternative to dislocation formation but the similarities in the effect and the role of dislocations and domain walls (both are discontinuous crystal "defects"), allows one to describe the domain structure effectively as a system of dislocations [5].

The most common model to calculate the critical thickness for strain relaxation of epitaxial layers on substrates, is the Matthews-Blakeslee model (MB) [2]. We will compare this with the People-Bean model (PB) [3], which

we believe is more appropriate for low-misfit perovskite ferroelectrics [55]. Both models have been developed to describe the appearance of dislocations in semiconductor layers. The MB model is known to predict too low values for the critical thickness, especially when high-quality substrate/film interfaces and low strains are involved. This is due to the fact that the assumptions of the MB model imply that interfacial misfit dislocations only form in the presence of grown-in threading dislocations [3]. For very small misfits, very few threading dislocations are expected and thus this mechanism is expected not to be a source of misfit dislocations. The PB model on the other hand, assumes no threading dislocations are present at first and these form when it is energetically favorable, purely based on an energy balance.

While for many cases, the MB model is very appropriate, the more phenomenological PB model has shown to explain experimental data for semiconductor films better. While more complete and complex models exist, we consider here the two models for which simple calculations, not requiring adjustable parameters, suffice and we compare the critical thicknesses H_c for the MB [46] and PB [56] models:

$$H_c^{MB} = \frac{b(1-\mu cos^2\beta)}{8\pi u_m(1+\nu)cos\lambda} ln(\frac{\alpha H_c}{b}) \tag{2.30}$$

$$H_c^{PB} = \frac{b(1-\mu)}{40\pi u_m^2(1+\nu)} ln(\frac{H_c}{b}) \tag{2.31}$$

with b the magnitude of the Burgers vector, u_m the misfit strain, ν the Poisson's ratio[6], α the cut-off parameter used to describe the continuum energy of the dislocation core, β the angle between the dislocation line and the Burgers vector, and λ the angle between the Burgers vector and the line that lies within the interface and in a plane normal to the dislocation line. These models will be used in chapter 4 to calculate the critical thicknesses for the involved film/substrate combination.

[6]Throughout this thesis, it is assumed that the Poisson's ratio of any thin film is equal to the bulk value of the material it consists of. This is not strictly true as has been shown by Biegalski et al. [57].

2.6.3 90° domains

At first sight, the domain structure of 90° domains is quite different from the 180° domain structure. The 90° domains are crystallographic a/c twins which share the (101)-plane as their low-strain plane. This gives rise to a domain wall close to the (101)-direction as indicated in Figure 2.8. Several models exist to describe the energetics of 90° domains. The simplest model balances the wall formation and elastic energies, giving

$$\begin{aligned} F_{wall} &= \frac{\sigma 2\sqrt{2}H}{D} \\ F_{elec} &= 0 \\ F_{elas} &= 2G(s_a - s_c)^2 D \end{aligned} \tag{2.32}$$

$$F_{total} = \frac{\sigma 2\sqrt{2}H}{D} + 2G(s_a - s_c)^2 D \tag{2.33}$$

Which can be minimized with respect to the domain width, resulting in:

$$D^2 = \frac{\sigma 2\sqrt{2}H}{2G(s_a - s_c)^2} \tag{2.34}$$

More realistic descriptions of the 90° domain structure, started with Roitburd [49], who considered an epitaxial thin film with 90° domains, on a substrate. Two cases are distinguished, namely when the thickness is (much) larger than the domain periodicity ($H \gg D$) and when the thickness is (much) smaller than the domain periodicity ($H \ll D$). Only when the thickness H is much larger than the domain periodicity D, an analytical solution could be found, which shows the same $D \sim \sqrt{H}$ relation as that of the cases described above.

As explained above, domain twinning takes place in order to attain coherence at the domain walls, by sharing the zero energy (101) plane. However, this is done at the expense of the coherence at the film-substrate interface. Speck and collaborators [4] proposed a way to solve that by creating arrays of dislocations/disclinations. Using that idea, since domain walls play the same role as dislocations, Pertsev and Zembilgotov [5] have modeled the stress fields in a thin film with 90° domains by fictitious dislocations. This

gives an expression of the internal energy as follows

$$\begin{aligned} F_{elas} &= \frac{GH}{1-\nu}(s_a^2 + 2\nu s_a s_c + s_c^2) \\ &+ \frac{GH}{1-\nu}(s_a - s_c)^2 \times \left[2\left((1+\nu)\frac{s_a}{s_a - s_c} - 1\right)\frac{d}{D} + \frac{D}{H} f_c\left(\frac{D}{H}, \frac{d}{D}\right)\right] \end{aligned} \tag{2.35}$$

$$\begin{aligned} F_{total} &= \frac{\sigma 2\sqrt{2}H}{D} + \frac{GH}{(1-\nu)}(s_a^2 + 2\nu s_a s_c + s_c^2) + \frac{GH}{(1-\nu)}(s_a - s_c)^2 \times \\ &\left[2\left((1+\nu)\frac{s_a}{s_a - s_c} - 1\right)\frac{d}{D} + \frac{D}{H} f_c\left(\frac{D}{H}, \frac{d}{D}\right)\right] \end{aligned} \tag{2.36}$$

Where s_a is the c-domain misfit (with the a-axis in-plane), s_c the a-domain misfit (with the c-axis in-plane) and f_c is a function of the two dimensionless variables defining the domain structure, $\frac{D}{H}$ and $\frac{d}{D}$ [5]. Minimalization with respect to the domain period, D, involves considerably more mathematics than the previous cases but it can be shown that it predicts a non-monotonic $D - H$ dependence for small thickness, H, a linear relation for intermediate H and a $D \sim \sqrt{H}$-dependence for large thicknesses. This will be treated in more detail in chapter 5.

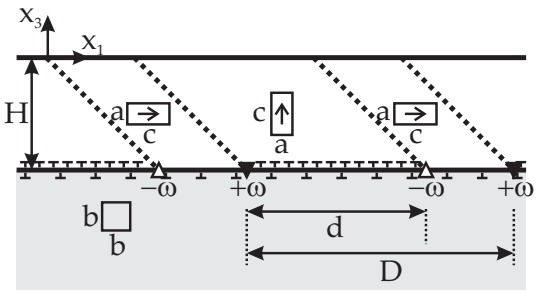

Figure 2.8: Schematic representation of the side-view of a 90° domain structure where the film/substrate misfit plays a key role. Within the structure, the main variables in the model of fictitious dislocations by Speck and collaborators [4] and Pertsev [5] is shown.